Article

Journal of the Brazilian Chemical Society

https://dx.doi.org/10.21577/0103-5053.20230162

J. Braz. Chem. Soc. **2024**, *35*, 4, e-20230162, 1-12

Development of an Electroanalytical Method for Ronidazole Determination in Environmental and Food Matrices Using Boron-Doped Diamond Electrode

Guilherme Bettio,[a] Leonardo L. Okumura,[a] Renê C. Silva[b] and Tiago A. Silva[*,a]

[a]*Departamento de Química, Universidade Federal de Viçosa, 36570-900 Viçosa-MG, Brazil*

[b]*Departamento de Física, Universidade Federal de Viçosa, 36570-900 Viçosa-MG, Brazil*

A novel electroanalytical approach is presented for the determination of ronidazole in environmental and food matrices by applying a cathodically pretreated boron-doped diamond electrode and the square-wave adsorptive cathodic stripping voltammetry technique. From the studies of cyclic voltammetry to investigate the electroactivity of the ronidazole molecule, the occurrence of an irreversible cathodic process was verified, which was more efficiently detected using the cathodically pretreated boron-doped diamond electrode compared to the anodically pretreated electrode. Still on the electrochemical response of ronidazole, the effects of pH and scan rate were studied and, its apparent diffusion coefficient was determined by chronoamperometry (8.20×10^{-6} cm^2 s^{-1}). Under optimal experimental conditions, the analytical curve obtained for ronidazole was linear in two concentration ranges (12.70 to 63.40 µmol L^{-1} and 76.04 to 126.2 µmol L^{-1}), with a limit of detection of 2.55 µmol L^{-1}. For intra- and inter-day repeatabilities, relative standard deviations of only 2.7 and 3.5% were verified, which demonstrated the stable analytical response of the electrode. Recovery percentages ranging from 96 to 100% were achieved in the analysis of natural water and whole milk samples. Therefore, the proposed electroanalytical method shows satisfactory analytical performance towards ronidazole determination in varied matrice samples.

Keywords: emerging contaminant, square-wave voltammetry, nitroimidazoles, boron-doped diamond electrode, water samples, milk analysis

Introduction

Emerging contaminants are a group of chemical compounds potentially toxic to human health and the environment.[1,2] Despite the growing number of publications on these micropollutants, they are rarely included in environmental monitoring legislation.[3,4] A worrying aspect of emerging contaminants is their continuous introduction into the environment, more specifically into water resources through domestic and industrial effluents.[4,5] Among the emerging contaminants, pharmaceuticals, and personal care products (PCPs) stand out,[6] and harmful effects can be seen even at low concentrations (ranging from µg L^{-1} to ng L^{-1}).[7]

Ronidazole (1-methyl-2-[(carbamoyloxy)methyl]-5-nitroimidazole, RNZ, Figure 1) is a compound of the class of nitroimidazoles, which are characterized by imidazole heterocycles containing a nitro functional group on the fifth carbon of the imidazole ring.[8] These compounds, as well as RNZ, are used as antibiotic and antiparasitic drugs in the treatment and prevention of veterinary diseases in poultry, cattle, and pigs.[9,10]

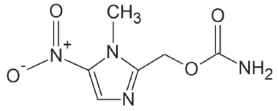

Figure 1. Molecular structure of ronidazole.

Due to the potential environmental impact and the carcinogenic and mutagenic action of nitroimidazoles,[11-13] their use has been banned in the European Union, United States of America, Japan, China and, more recently, in Brazil.[14] Despite the ban imposed by regulatory authorities, the illegal use of RNZ and other nitroimidazoles is still observed.[14] Nitroimidazoles have already been determined in food samples (for example, honey,[15] turkey muscle,[16] swine tissues,[17] milk[18] and egg[19]) and in water samples.[20-23]

*e-mail: tiago.a.silva@ufv.br
Editor handled this article: Rodrigo A. A. Muñoz (Associate)
This manuscript is part of a series of publications in the Journal of the Brazilian Chemical Society by young researchers who work in Brazil or have a solid scientific connection with our country. The JBCS welcomes these young investigators who brighten the future of chemical sciences.

Contamination of water resources with antibiotics such as RNZ can occur through different routes, such as hospital waste, pharmaceutical plants, domestic sewage or farms dedicated to livestock.[22] Therefore, nitroimidazole residues are associated with environmental impacts and food and beverage contamination, and new analytical methods are required for monitoring RNZ in water and food products.

A set of analytical methods for the determination of RNZ are available, including liquid chromatography-tandem mass spectrometry (LC-MS/MS),[24,25] enzyme-linked immuno-sorbent assay (ELISA),[26,27] gas chromatography (GC),[28] high-performance liquid chromatography with ultraviolet detection (HPLC-UV).[29,30] Although these methods are efficient due to the low limits of detection and quantification, robustness and analytical reliability, there are some disadvantages, such as long analysis time, excessive use of organic solvents and, equipment incompatibility with portability and miniaturization.[31] To overcome the limitations of conventional methods of analysis, electrochemical methods emerge as an alternative analytical tool.[32,33] Electrochemical methods are developed by applying electrochemical sensors, which need to provide fast and simple analytical tests for the determination of relevant chemical species at low concentration.[34] The applicability of these devices in analytical routines enables data collection with minimal alteration and manipulation of samples.[35] So far, four works have been reported in the literature for the electroanalytical determination of RNZ, using differential pulse polarography[36] and bare[37] or modified glassy carbon electrodes with differential pulse voltammetric[38] or amperometric[39] detection.

An electrode material that has stood out in the context of the development of new electroanalytical methods is the boron-doped diamond (BDD). BDD films are prepared via chemical vapor deposition (CVD), with the diamond structure being formed together with a dopant agent (boron). This process makes it possible to manipulate the physical and chemical properties of BDD, e.g., attributing electrical conductivity to the film.[40] The BDD presents a polycrystalline lattice consisting mainly of sp^2 carbons and boron in the interstices. The surface features an outer layer with endings of hydrogen atoms. BDD films have been widely used in the development of electrochemical methods,[41] being referred to as boron-doped diamond electrodes. For applications as electrochemical sensors, BDD electrodes present a number of favorable features, including low and stable background current, weak adsorption of polar and non-polar molecules, low passivation, high stability of electrochemical response at different measurement environments and wide potential window.[42,43] From these properties, some featured applications of BDD as electrochemical sensors include the determination of different target compounds of pharmaceutical,[44-46] environmental[47,48] and biological[49,50] interest, among others.

In this work, the electrochemical and analytical characteristics of BDD electrodes were explored for the first time to study the redox behavior of RNZ and perform its voltammetric determination in natural water and milk samples.

Experimental

Reagents, solutions, and samples

All reagents were of analytical grade and all solutions were prepared with ultrapure water supplied by a Millipore Milli-Q system (resistivity > 18 MΩ cm, 25 ºC). NaH_2PO_4, Na_2HPO_4, Na_3PO_4 and $K_4[Fe(CN)_6]$ were purchased from Synth (São Paulo, Brazil). HNO_3 (65.0%), H_2SO_4 (98.0%), KCl, $MgSO_4$, CH_3COONa and H_3PO_4 (85.0%) were obtained from Vetec (São Paulo, Brazil). Acetonitrile was purchased from Merck (Darmstadt, Germany). RNZ was acquired by Sigma-Aldrich (São Paulo, Brazil) as an analytical standard. A 1.2×10^{-2} mol L^{-1} RNZ standard stock solution was prepared using acetonitrile as solvent and stored at 4 ºC. Aqueous supporting electrolyte solutions of 0.1 mol L^{-1} phosphate buffer with pH ranging from 2.0 to 12.0 were prepared. For convenience, all the phosphate solutions with pH ranging from 2.0 to 12.0 are assigned as a buffer solution in this work, however, the reader should be aware that the phosphate-buffer system has buffering capacity only in the pH ranges of ±1.0 around their respective pK_a values (2.14, 7.20 and 12.34).

A sterile polyethylene terephthalate (PET) flask was used for sampling the natural waters. Natural water samples were collected in the lake of the Federal University of Viçosa (Brazil). Before analysis, samples were filtered using a quantitative filter (diameter of 125 mm) to remove suspended particles and, then, enriched by dissolving adequate amounts of the respective salts to obtain the 0.10 mol L^{-1} phosphate buffer (pH = 7.0) constituting the optimum supporting electrolyte.

The whole milk sample was purchased at the local market. For preparing this sample, the "quick, easy, cheap, effective, rugged and safe" (QuEChERS) method was applied.[51,52] Thus, in a Falcon tube, 5.0 mL of milk sample and 5.0 mL of acetonitrile were transferred. The mixture was vortexed for about 1 min. After adding 2.0 g of magnesium sulfate and 0.70 g of sodium acetate, vortexing was performed again for the same period. These processes correspond, respectively, to the extraction and partition steps. Before starting the

cleaning step, the mixture was centrifuged at 4000 rpm for 5 min. The supernatant, collected after centrifugation, was drawn through a syringe against a 0.50 μm syringe filter. The filtrate was quantitatively transferred to a 10 mL flask, and the volume was completed with the supporting electrolyte solution (0.10 mol L^{-1} phosphate buffer, pH = 7.0).

Instrumentation

All voltammetric measurements were carried out in a PGSTAT 128 N Autolab potentiostat/galvanostat Eco-Chemie (Herisau, Switzerland) interfaced to a computer and managed with NOVA software (version 1.11). It was used a 50 mL conventional three-electrode electrochemical cell consisting of BDD as working electrode, platinum wire as auxiliary electrode and Ag/AgCl (3.0 mol L^{-1} KCl) as reference electrode. Scanning electron microscopy (SEM) was carried out using a JEOL model JSM-6010 LA operating at 15 kV (Tokyo, Japan).

BDD pretreatment

The BDD film was synthesized on silicon wafers and with a boron content of 8000 ppm in the Centre Suisse d'Electronique et de Microtechnique SA (CSEM), Neuchâtel, Switzerland, using the hot filament chemical vapor deposition technique. For use as working electrode, the conducting silicon wafer substrate supporting the BDD film was fixed to a copper plate using tin solder and sealed with epoxy resin, leaving free only the BDD surface (exposed geometric area of 0.16 cm^2). Prior to the electrochemical measurements with the $[Fe(CN)_6]^{3-/4-}$ redox probe or RNZ analyte, the BDD electrode was subjected to anodic pretreatment (APT-BDD) or cathodic pretreatment (CPT-BDD).[53,54] Both were carried out at 0.50 mol L^{-1} H_2SO_4 adopting chronoamperometry with the following conditions: in APT-BDD the electrode was subjected to cathodic polarization (−3.0 V; 120 s), followed by anodic polarization (+3.0 V; 120 s); in CPT-BDD the electrode was subjected to anodic polarization (+3.0 V; 120 s), followed by cathodic polarization (−3.0 V; 120 s).

Analytical procedures for ronidazole determination

The electrochemical behavior of RNZ was studied by cyclic voltammetry, while in the analytical assays the square-wave voltammetry (SWV) and square-wave adsorptive cathodic stripping voltammetry (SWAdCSV) techniques were used.

After confirming the electroactivity of the RNZ molecule on the BDD surface, the electrochemical properties of the analyte were investigated, and an electroanalytical method was developed for the determination of RNZ in an environmental sample (lake water) and food sample (whole milk). For the development of the voltammetric method, the surface terminations of the BDD (pretreatment), the pH of supporting electrolyte and the operational parameters of the SWAdCSV (amplitude (a), frequency (f), accumulation potential (E_{acc}) and accumulation time (t_{acc})) were optimized. In the case of pH of supporting electrolyte, this parameter was varied in the range of 2.0 to 12.0 using 0.10 mol L^{-1} phosphate buffer solutions; regarding the SWAdCSV parameters, these were evaluated in the following ranges: amplitude (10 to 140 mV), frequency (5 to 50 Hz), accumulation potential (−0.2 to +1.0 V) and accumulation time (30 to 150 s).

For the analytical characterization of the proposed method, an analytical curve was constructed from successive additions of aliquots of a 1.2×10^{-3} mol L^{-1} RNZ standard solution in the electrochemical cell containing previously the optimum supporting electrolyte solution (0.10 mol L^{-1} phosphate buffer, pH = 7.0). From the obtained analytical curve, the following analytical parameters were recorded: sensitivity (slope of the analytical curve), linear dynamic range and limit of detection (LOD). All voltammetric measurements were made in triplicate. The analytical method was applied by recovery tests. Natural lake water and milk samples were enriched with RNZ standard at two different concentration levels (38.0 and 88.0 μmol L^{-1}) for this purpose. The milk sample after going through the QuEChERS method process was diluted by a factor of 2 with the supporting electrolyte solution (0.10 mol L^{-1} phosphate buffer, pH = 7.0) to then be analyzed by the voltammetric method. On the other hand, no dilution was performed in the case of the lake water sample; in this case, the supporting electrolyte salts were directly added to the lake water sample to achieve the desired concentration and buffer pH (i.e., 0.10 mol L^{-1} phosphate buffer, pH = 7.0). The recovered concentration was obtained by interpolating the analytical signal recorded for the enriched samples in the analytical curve equation.

Results and Discussion

Morphological and electrochemical characterization of BDD

The morphological features of the BDD surface before and after the performed electrochemical pretreatments were evaluated by SEM. Figures 2a-2c provide the SEM images collected for the as-received BDD, APT-BDD and CPT-BDD. Thus, a pyramidal structure was verified, which is typical for BDD films, with the presence of grains

with size < 1 μm, suggesting that the boron doping of the crystalline structure of diamond is high.[55] It is expected that the high degree of doping may contribute to a fast electrochemical response.[56] In addition, from Figures 2b and 2c it is evident that these structural and morphological features were not lost after performing the anodic and cathodic electrochemical pretreatments. The non-apparent BDD surface degradation after anodic and cathodic pretreatment on the applied conditions was also verified by other authors such Salazar-Banda *et al*.[54] and Duo *et al*.[57]

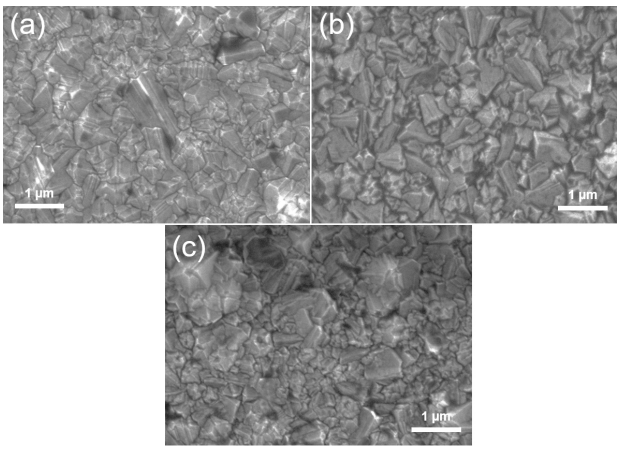

Figure 2. SEM micrograph of the (a) as-received BDD, (b) APT-BDD and (c) CPT-BDD electrode surface.

The electrochemical behavior of BDD electrodes is strongly influenced by the terminal chemistry of its surface, which can be easily modulated by electrochemical pretreatments. The electrochemical BDD pretreatment conducted in an acid medium can provide a surface with predominant termination in hydrogen or oxygen; in this sense, hydrogen-terminated BDD is obtained via cathodic pretreatment and oxygenated groups-terminated surface via anodic pretreatment. Thus, it becomes relevant to evaluate the electrochemical behavior of BDD submitted to both pretreatments. The electrochemical properties of the BDD used in this study were investigated through the charge transfer kinetic of the $[Fe(CN)_6]^{3-}/[Fe(CN)_6]^{4-}$ redox couple according to the pretreatment (anodic or cathodic). Cyclic voltammograms of as-received BDD, APT-BDD and CPT-BDD pretreated BDD are shown in Figure 3a.

The as-received-BDD showed a similar voltammetric profile to the CPT-BDD. Both exhibited marked electrochemical responses in terms of anodic (j_{pa}) and cathodic (j_{pc}) peak current densities and reversibility since the peak-to-peak potential separations (ΔE_p) between the anodic (E_{pa}) and cathodic (E_{pc}) peak potentials ($\Delta E_p = E_{pa} - E_{pc}$) were narrow. Table 1 brings a set of electrochemical parameters obtained for BDD under all evaluated conditions (as-received, APT and CPT). Thus, the peak current density ratio (j_{pa}/j_{pc}) was equal to 0.884 for the as-received-BDD and 1.00 for both pretreated electrodes, respectively. On the other hand, regarding the ΔE_p parameter, the redox probe exhibited a *quasi*-reversible behavior over APT-BDD (Figure 3a) with ΔE_p = 515 mV, that is, almost 8 times greater than the value recorded for the CPT-BDD electrode. Results obtained for the redox probe in an acid medium demonstrate that the BDD submitted to a cathodic pretreatment presents superior electrochemical characteristics. Furthermore, by the similarity of the voltammetric profile, the as-received BDD presented a preferential termination in hydrogen, however, for a control of this termination, the electrochemical pretreatment is necessary to obtain a reversible behavior.

The verified results are fully in agreement with the literature dedicated to the study of BDD electrodes with the chosen redox probe.[54,57-61] The predominance of oxygen endings on the surface of APT-BDD can be associated with a greater degree of irreversibility and lower electrochemical response towards the $[Fe(CN)_6^3]^-/[Fe(CN)_6]^{4-}$ redox probe. It is expected that the electron transfer kinetic of this redox couple decreases by interacting with a negatively charged surface generated by oxygenated functional groups attached to the electrode surface.[61] In the case of CPT-BDD, the H-branches facilitate the electronic transfer process of the redox couple on the electrode surface, which favors a high peak current and electrochemical reversibility.[58]

To determine the electroactive surface area of as-received BDD, APT-BDD and CPT-BDD, cyclic voltammetry assays at different scan rates (v) were carried out using the same redox probe. The cyclic voltammograms obtained using all the electrodes (as-received BDD, ATP-BDD and CPT-BDD) in the scan rate range of 10 to 300 mV s^{-1} are displayed in Figures S1a, S1c and S1e (Supplementary Information (SI) section). As expected, the peak currents increased in intensity with the increase of scan rate, with a linear relationship between the anodic peak current and the square root of the scan rate (plots of I_{pa} *vs.* $v^{1/2}$ shown in Figures S1b, S1d and S1f). Linear relationships for I_{pa} *vs.* $v^{1/2}$ demonstrate that the redox process was controlled by diffusional mass transport, according to the theoretical Randles-Sevcik equation for a reversible and diffusion-controlled process, equation 1:

$$I_p = \pm(2.69 \times 10^5)n^{3/2}AD^{1/2}Cv^{1/2} \quad (1)$$

where I_p is the anodic or cathodic peak current (in Amperes), n is the number of electrons in the redox reaction (n = 1), A is the electroactive area (in cm^2), D is the

diffusion coefficient (1.87×10^{-6} cm^2 s^{-1} for the $[Fe(CN)_6]^{4-}$ species in 0.5 mol L^{-1} H_2SO_4),[62] *C* is the concentration of the electroactive specie (1.0×10^{-6} mol cm^{-3}) and $v^{1/2}$, as already mentioned, is the square root of the potential scan rate (in V$^{1/2}$ s$^{-1/2}$). Considering the mathematical relationship between I_p and $v^{1/2}$ established by the Randles-Sevcik equation and the experimental slopes of the I_{pa} *vs.* $v^{1/2}$ curves (Figures S1b, S1d and S1f), the respective electroactive areas were estimated, and the obtained values are provided in Table 1. Therefore, the APT-BDD presented an electroactive surface area of 0.073 cm^2, while the as-received BDD and CPT-BDD presented electroactive areas of 0.098 and 0.113 cm^2, respectively. The electroactive areas were all smaller than the geometric area of the used BDD electrode. The justification for this difference can be found in the work reported by Holt *et al.*,[63] according to which this difference stems from the non-uniformity of the distribution of boron atoms (B) on the surface of the electrode, since it depends on the level of doping with boron, and the conductive areas are those that coincide with B atoms located on the surface.

To investigate in more details the charge transfer kinetic features of the BDD electrode subject to the applied pretreatments, electrochemical impedance spectroscopy (EIS) tests were conducted. The Nyquist diagrams obtained for the same $[Fe(CN)_6]^{3-}/[Fe(CN)_6]^{4-}$ redox probe in acid medium using as-received BDD, APT-BDD and CPT-BDD are displayed in Figure 3b. As expected, a semicircle in the high frequency region related to the charge transfer resistance was obtained in all cases. To extract quantitative data from the respective Nyquist diagrams, the Randles equivalent circuit shown in the inset of Figure 3b was fitted to the experimental data, including the following elements: resistance of the supporting electrolyte solution (R_s) in series with the parallel combination of the double-layer capacitance (C_{dl}), charge-transfer resistance (R_{ct}) and Warburg impedance (Z_W). From this, the R_{ct} values reported in Table 1 were obtained, demonstrating that the anodically treated surface presented the worst charge transfer kinetics. Still with the impedance data, it was possible to estimate the heterogeneous electron transfer rate constant (k^0) for all electrodes studied by using equation 2:[64]

$$k^0 = \frac{RT}{F^2 R_{ct} A C} \quad (2)$$

where R is the universal gas constant (8.314 J K^{-1} mol^{-1}), T is the thermodynamic temperature (298.15 K), F is the Faraday constant (96485 C mol^{-1}), and the other terms have already been defined. Thus, the k^0 constant assumed the values shown in Table 1. It was evident that carrying out the cathodic pretreatment of the BDD surface is essential to guarantee adequate charge transfer kinetics. First, as also verified by Suffredini *et al.*,[59] the charge transfer

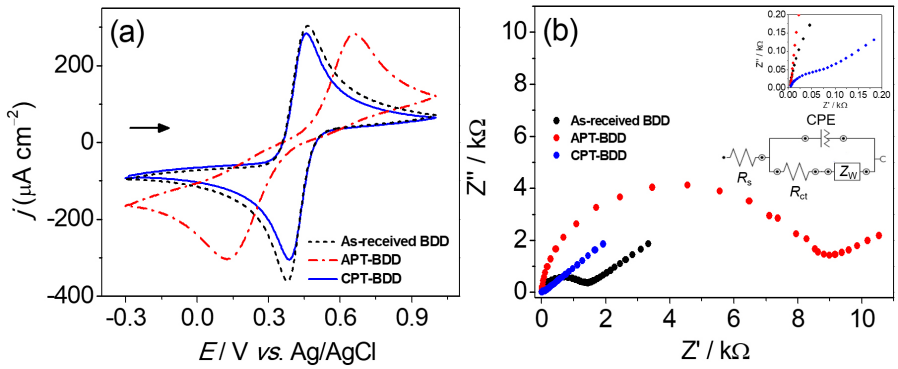

Figure 3. (a) Cyclic voltammograms and (b) Nyquist plots recorded in 0.5 mol L^{-1} H_2SO_4 containing 1.0×10^{-3} mol L^{-1} $K_4Fe(CN)_6$ using as-received BDD, APT-BDD and CPT-BDD electrode (inset: Randles equivalent circuit). Cyclic voltammetry scan rate (v) = 50 mV s^{-1}; EIS conditions: applied potential = half-wave potential, frequency range: 100 kHz to 100 mHz and amplitude = 10 mV.

Table 1. Electrochemical parameters recorded from the cyclic voltammograms and Nyquist plots of as-received BDD, APT-BDD and CPT-BDD

Electrode	ΔE_p[a] / mV	j_{pa}/j_{pc} ratio[a]	A / cm^2	R_{ct} / kΩ	k^0 / (cm s^{-1})
As-received	81	0.884	0.098	1.42	1.17×10^{-3}
APT-BDD	515	1.00	0.073	8.97	1.86×10^{-4}
CPT-BDD	66	1.00	0.113	0.11	1.50×10^{-2}

[a]At scan rate = 50 mV s^{-1}. ΔE_p: peak-to-peak potential separation between the anodic (E_{pa}) and cathodic (E_{pc}) peak potential ($\Delta E_p = E_{pa} - E_{pc}$); j_{pa}: anodic peak current density; j_{pc}: cathodic peak current density; A: electroactive surface area; R_{ct}: charge-transfer resistance; k^0: heterogeneous electron transfer rate constant.

kinetics for the studied redox probe was slow with the anodically treated BDD electrode, which also corroborates the cyclic voltammetry data presented before. In addition, although the electrochemical behavior of the as-received and cathodically pretreated electrodes were quite similar when evaluated by cyclic voltammetry, the impedance data made it possible to demonstrate that it is indeed necessary to pretreat the BDD electrode, with an increase of almost 10 times in the k^0 constant when passing from the as-received BDD to the CPT-BDD electrode.

Electrochemical response of RNZ

According to the molecular structure of RNZ (Figure 1), there is the presence of nitrogenous groups, which may be involved in redox processes. Furthermore, the RNZ electrochemical response on BDD can be affected by the surface termination of this electrode. In this way, the RNZ electrochemical activity was investigated by cyclic voltammetry on both APT-BDD and CPT-BDD electrodes.

Figure 4 displays the cyclic voltammograms recorded in phosphate buffer solution in the presence of RNZ. Cyclic voltamograms obtained only in supporting electrolyte (blank) can be seen in Figure S2 (SI section), with the absence of any faradaic peak as desired. Thus, in presence of RNZ, a sharp cathodic peak was verified during the cathodic potential scanning, without the occurrence of anodic peaks after the inversion of the potential scanning direction. This finding demonstrated that the RNZ underwent an irreversible reduction reaction on both pretreated BDD. The RNZ reduction was positioned at –0.85, –0.76 and –0.67 V on as-received BDD, APT-BDD and CPT-BDD, respectively. Regarding the cathodic peak current density (j_{pc}), this was more pronounced with the use of CPT-BDD compared to as-received BDD and APT-BDD, being, in fact around 30% higher. This pronounced increase in the peak current density suggests that the CPT-BDD could contribute to greater analytical sensitivity of the method under development. The best performance of the cathodically pretreated surface can be understood by considering the surface characteristics of the BDD electrode and the molecular structure of the RNZ. The surface of CPT-BDD is predominantly hydrophobic and highly conductive, while APT-BDD is hydrophilic, less conductive and rich in negatively charged oxygen groups.[65] RNZ has a pK_a = 1.32[37] and thus the fully deprotonated form predominates in the used pH condition (pH 6.5). Therefore, the better voltammetric response of RNZ on CPT-BDD can be associated with the better electrical conductivity of this electrode and also with the minimization of electrostatic repulsion interactions between electronegative atoms present in the RNZ structure (N and O) and the oxygenated functional groups present on the surface of APT-BDD.

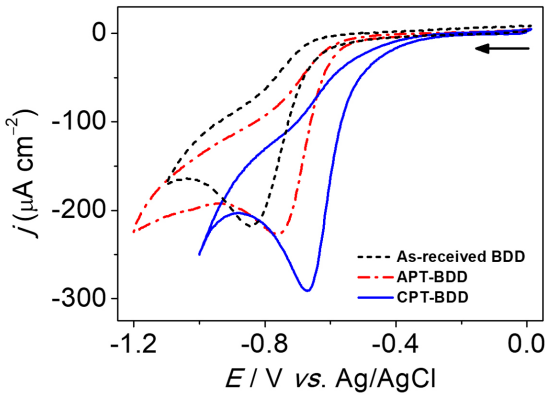

Figure 4. Cyclic voltammograms recorded in 0.1 mol L^{-1} phosphate buffer solution (pH = 6.5) containing 5.0×10^{-5} mol L^{-1} RNZ using as-received BDD, APT-BDD and CPT-BDD electrode. v = 50 mV s^{-1}.

In order to study the effective influence of the BDD surface termination on the electrochemical response and the analytical capacity of this electrode regarding the RNZ voltammetric determination, preliminary analytical curves were constructed using the as-received BDD, APT-BDD and CPT-BDD electrodes and SWV.

In Figures S3A-S3C (SI section), the square-wave voltammograms recorded at different RNZ concentrations by applying as-received BDD, APT-BDD and CPT-BDD electrodes are provided. The analytical curves (plots of $-I_{pc}$ *vs.* c(RNZ)) were constructed from the respective cathodic peak currents (I_{pc}) and are shown in Figure S3D. Firstly, the voltammograms in Figures S3A-S3C corroborate to what was noticed in the cyclic voltammetry (Figure 4), i.e., the cathodic peak potential for RNZ was more negative on the as-received BDD and APT-BDD, while CPT-BDD exhibited more intense peak currents. However, as shown in Figure S3D, all the BDD surfaces provided similar analytical sensitivities (slope of the analytical curve) towards RNZ determination in this preliminary analytical study: 0.098 (as-received BDD), 0.108 (APT-BDD) and 0.112 μA L $μmol^{-1}$ (CPT-BDD), respectively. Comparatively, therefore, there was an increase of only 10% with the use of the CPT-BDD electrode. This is a very interesting finding, which allows emphasizing that increases in the analytical signal obtained in previous studies of cyclic voltammetry are not always sufficient to infer the best analytical performance of an electrochemical sensor. In view of this, given the effects of displacement of the cathodic peak potential to a region closer to zero, subsequent studies for the quantification of RNZ focused on the use of the CPT-BDD.

Cyclic voltammetry scan rate study for RNZ at CPT-BDD

The evaluation of the peak current variation according to the potential scan rate in cyclic voltammetry measurements is an important tool to obtain additional information on the redox process under study. In this sense, cyclic voltammograms were recorded in the scan rate range of 10 to 75 mV s^{-1}, and the recorded voltammograms are shown in Figure S4a (SI section). Thus, it was found that the cathodic peak potential tended towards more negative values as the scan rate increased, with this displacement of the peak potential being characteristic of irreversible redox processes. From the cyclic voltammograms in Figure S4a, the plots of I_{pc} *vs.* $v^{1/2}$ and log $-I_{pc}$ *vs.* log *v* were constructed, and these can be seen in Figures S4b and S4c (SI section). Based on the correlation coefficient (r = 0.998), I_{pc} presented a linear dependence with the square root of the scan rate, as shown in Figure S4b; which suggests that the RNZ reduction on the CPT-BDD surface was a diffusion-controlled redox process. It should be noted, however, that the linear coefficient of the regression equation: I_{pc} / μA = –0.895 $v^{1/2}$ / (mV$^{1/2}$ $s^{-1/2}$) – 9.64 μA was different from zero, indicating the occurrence of a weak absorptive process on the surface of the electrode. This fact is confirmed by the linear relationship between log $-I_{pc}$ and log *v* (Figure S3c), with a slope of 0.599. This experimental slope for the log $-I_{pc}$ *vs.* log *v* was close to the reference value for diffusion-controlled electrochemical processes (0.50),[66] which reinforces the predominance of diffusion.

Chronoamperometric determination of the apparent diffusion coefficient for RNZ

Considering the predominance of diffusional mass transport in controlling the RNZ voltammetric response on the BDD surface, a chronoamperometric study was carried out to determine the apparent diffusion coefficient (D_{app}) of this molecule in the used supporting electrolyte solution. Thus, in Figure 5A the chronoamperograms recorded towards different RNZ concentrations are presented, with the measurements performed by stepping the potential from 0.0 V (without any faradaic process) to –0.7 V. With this potential step, the cathodic current increased due to the RNZ reduction reaction, which decreased with time. From the currents measured in the final seconds of each experiment, a plot of background-corrected current (subtraction of capacitive current) *versus* the inverse of the square root of time was constructed for each RNZ concentration. The obtained I *vs.* $t^{-1/2}$ curves are shown in Figure 5B and linear relationships were observed in all cases. Therefore, the expected behavior for processes controlled by linear diffusion represented by Cottrell's equation was obtained. Cottrell's equation establishes the linear relationship between I and $t^{-1/2}$, as shown in equation 3:

$$I = \frac{nFAD^{1/2}c}{\mu^{1/2}t^{1/2}} \quad (3)$$

where t is the elapsed interval time, n is the number of electrons transferred in the redox process, F is the Faraday constant, D is the diffusion coefficient of the electroactive species in the considered supporting electrolyte and *c* is the concentration of the electroactive species. Taking into account the slopes of the I *vs.* $t^{-1/2}$ curves obtained for each RNZ concentration, and naming them with k, a last plot relating the k slopes to the RNZ concentration (*c*(RNZ)) was constructed (Figure 5C). In this case, the determined linear relationship obeyed the following linear regression equation, equation 4:

$$k / (\mu A\ s^{1/2}) = -1.16\ c(RNZ) / (nmol\ cm^{-3}) + 1.66\ \mu A\ s^{1/2},\ r = 0.998 \quad (4)$$

Comparing the slope of the experimental (k slopes) *vs.* *c*(RNZ) curve with the theoretical slope of Cottrell's equation (theoretical k = $nFAD^{1/2}/\pi^{1/2}$, equation 3), the apparent diffusion coefficient of RNZ in 0.1 mol L^{-1} phosphate buffer solution (pH = 6.5) was predicted as 8.20×10^{-6} cm^2 s^{-1}. For the calculation of D_{app}, a n = 4 was considered, according to the probable redox mechanism previously proposed by Stanley *et al.*[39] and schematically represented in Figure 6 involving the reduction of the nitro group of RNZ molecule to the corresponding hydroxylamine derivative.

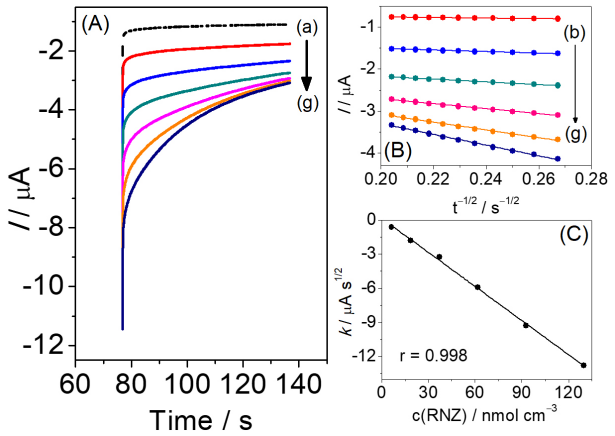

Figure 5. (A) Chronoamperometric curves recorded in 0.1 mol L^{-1} phosphate buffer solution (pH = 6.5) at different RNZ concentrations: (a) 0.00 (dashed line); (b) 6.19; (c) 18.6; (d) 37.1; (e) 61.8; (f) 92.7 and (g) 129 μmol L^{-1}. Applied step potential: 0.0 to –0.7 V *vs.* Ag/AgCl (3.0 mol L^{-1} KCl). Plots of the (B) background-corrected cathodic current (I) *vs.* $t^{-1/2}$ for each RNZ concentration and (C) slopes of I *vs.* $t^{-1/2}$ curves *vs.* *c*(RNZ).

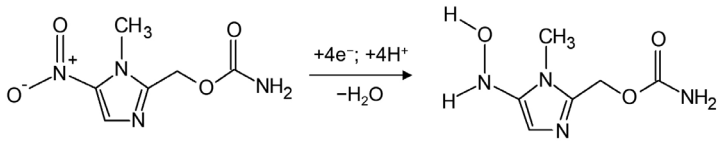

Figure 6. Schematic representation of the probable RNZ reduction reaction.

Optimizations

pH of supporting electrolyte

The effect of the pH of supporting electrolyte on the RNZ voltammetric response was evaluated from SWV measurements conducted in 0.1 mol L^{-1} phosphate buffer solutions with pH ranging of 2.0 to 12.0. In Figure S5a (SI section), the SW voltammograms recorded in this pH range are presented, being readily observed the great influence of pH on the cathodic response of RNZ. In fact, at acid condition, a discrete cathodic peak was verified for the RNZ molecule, with an increase in the electrochemical response according to the elevation in pH. According to the calculations of species distribution as a function of pH reported by Diniz *et al.*,[37] RNZ has a pK_a = 1.32, and from that, the deprotonated and electroactive form of RNZ will predominate at pH > 2.5 (α_1 > 0.9). Therefore, it is understandable that the RNZ showed a poor response in an acid medium, specifically at pH = 2.0. In analytical terms, the selection of the pH should be carried out by observing the recording of the most intense peak current possible. In this sense, in the pH range 7-12, I_{pc} values around 10 µA were obtained (Figure S5b). As the I_{pc} was maximum at pH 7-8, the pH = 7.0 condition was selected for further analytical studies, since this condition should be closer to the pH verified for the target samples (natural waters and treated milk). Therefore, all subsequent studies were conducted using 0.10 mol L^{-1} phosphate buffer solution (pH = 7.0) as the supporting electrolyte.

SWAdCSV parameters

The instrumental parameters of the voltammetric technique influencing the RNZ detection were also subjected to optimization. In this way, the I_{pc} analytical signal can be amplified from parameter optimization, to contribute to greater sensitivity of the electrochemical method. Initially, the frequency and amplitude of SWV were optimized. In Figures S6a and S6b (SI section) are displayed the recorded square-wave voltammograms and in Figures S7a and S7b (SI section) variations of peak current and of peak width half are presented as a function of amplitude and frequency. The selection of optimal amplitude and frequency conditions took into account the compromise between a high peak current and narrow peak width half. From this, the optimal amplitude and frequency conditions were defined as: f = 10 Hz and a = 80 mV.

Subsequently, it was verified that the application of an analyte pre-accumulation step resulted in a higher I_{pc} value in relation to the direct SWV analysis (without pre-accumulation). The voltammograms in Figure 7 show that the cathodic peak current was about twice as intense with the application of the pre-accumulation step. Thus, it was decided to employ the SWAdCSV technique and, therefore, technical parameters of the pre-accumulation step were also optimized, i.e., pre-accumulation potential and time. As can be seen in Figures S6d and S7d, there was no significant difference in the electrochemical response for different E_{acc} values, varied in the range of −0.20 to +1.0 V, respectively. A similar behavior was noted in relation to t_{acc} (Figures S6c and S7c), i.e., I_{pc} was practically the same for different t_{acc} values (ranging from 30 to 150 s), suggesting that the electrode surface is quickly saturated by the analyte molecules, which is very interesting for decreasing the analysis time. Therefore, the SWAdCSV method was then employed with the following parameters for the pre-accumulation step: E_{acc} = 0.00 V and t_{acc} = 30 s.

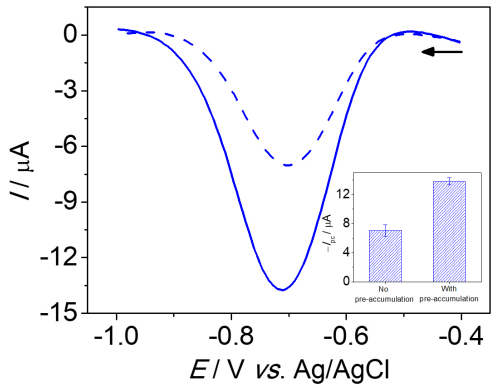

Figure 7. Comparison of SWVs recorded for RNZ with (full line) and without (dashed line) pre-accumulation (conditions: 0.0 V by 30 s). Inset: cathodic peak currents obtained for RNZ with and without pre-accumulation.

Analytical features

From the optimized experimental conditions of SWAdCSV and confirmation of the effectiveness of using the CPT-BDD in the monitoring of RNZ reduction, the analytical curve was constructed according to I_{pc} analytical signal generated by successive additions of RNZ standard solution in the electrochemical cell

containing the supporting electrolyte solution. The SWAdCS voltammograms recorded over the different RNZ concentrations, as well as the obtained analytical curve are displayed in Figure 8.

Based on the obtained analytical curve (inset of Figure 8), the RNZ voltammetric response varied linearly in two concentration ranges: 12.70 to 63.40 μmol L^{-1} and 76.04 to 126.2 μmol L^{-1}. The first concentration range obeyed the following linear regression equation: $I_{pc}/\mu A = -(0.15 \pm 0.07)\, c(RNZ)/\mu mol\, L^{-1} + (0.24 \pm 0.01)\, \mu A$, r = 0.997; and in the case of the second concentration range, the corresponding linear regression equation was: I_{pc} / μA = −(0.088 ± 0.001) *c*(RNZ) + (4.0 ± 0.2) μA, with r = 0.999. The LOD was experimentally determined as the RNZ concentration providing a detectable and reproducible change of baseline comparatively to blank solution (i.e., only supporting electrolyte). From that, a LOD of 2.55 μmol L^{-1} was obtained.

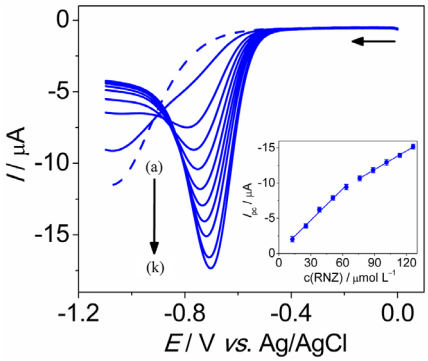

Figure 8. SWAdCS voltammograms recorded using CPT-BDD electrode in 0.1 mol L^{-1} phosphate buffer solution (pH = 7.0) in the presence of different RNZ concentrations: (a) 0.00 (blank); (b) 12.7; (c) 25.4; (d) 38.1; (e) 50.8; (f) 63.4; (g) 76.0; (h) 88.6; (i) 101.2; (j) 113.7 and (k) 126.2 μmol L^{-1}. SWAdCSV parameters: *f* = 10 Hz; a = 80 mV; E_{acc} = 0.0 V; t_{acc} = 30 s. Inset: analytical curve (I_{pc} *vs.* *c*(RNZ)).

Table 2 shows a comparison between the proposed method and other methods based on an electrochemical sensor for RNZ determination. The proposed method presents a wide linear range of response in the order of μmol L^{-1}, as observed in the other compared methods. It is important to emphasize that, despite the LOD in the order of nmol L^{-1}, the methods based on the modified glassy carbon electrodes sensors were applied at the RNZ quantifications in the order of μmol L^{-1}. The developed method based on CPT-BDD electrode provided a LOD in the same concentration order (μmol L^{-1}) as the linear response range. Additionally, we need to emphasize that the BDD electrode used is obtained from commercial sources, therefore, manufactured under a consolidated industrial process, and can be used directly without any additional modification on a laboratory scale as in the case of the previously reported electrodes. These characteristics of the BDD electrode provide the developed method with great operational ease and the possibility of widespread use.

Repeatability and selectivity studies

The precision of measurement of the CPT-BDD electrode was evaluated by intra-day and inter-day repeatability tests. In the case of intra-day repeatability, 10 successive SWAdCSV measurements were taken (n = 10), while for inter-day repeatability, the RNZ response measured on three different days was compared (n = 3). Voltamograms recorded in each study are shown in Figures S8a and S8b (SI section). For intra-day repeatability the relative standard deviation (RSD) was only 2.7%, and in the case of inter-day repeatability an RSD of 3.5% was verified. Both RSD values demonstrated that a stable analytical response was provided by the CPT-BDD, ensuring that the proposed analytical method has excellent precision in detecting RNZ.

The selectivity of the CPT-BDD electrode towards RNZ detection was tested by performing SWAdCSV measurements in the absence and presence of other antibiotics (ciprofloxacin and isoniazid) at analyte:interferent concentration ratios of 1:1 and 1:10. The cathodic peak current results obtained are organized in Figure S9 (SI section). As can be seen, both antibiotics did not significantly interfere with the analytical signal verified for the RNZ, with relative errors lower than 2.9%.

Table 2. Comparison of analytical parameters for the voltammetric determination of RNZ

Electrode	Technique	Linear range / (μmol L^{-1})	Sensitivity / (μA L μmol^{-1} cm^{-2})	LOD / (μmol L^{-1})	Reference
$CoCo_2O_4$ NRs/h-BN/GCE	DPV	0.01 to 10.41 and 12.81 to 1345.4	5.845	0.003	38
GCE-MoN@GA	amperometry	0.001 to 918.44	78.65	0.0013	39
CPT-BDD	SWAdCSV	12.7 to 63.4 and 76.0 to 126.2	1.33 (1st linear range) and 0.779 (2nd linear range)	2.55	this work

GCE-MoN@GA: glassy carbon electrode and molybdenum nitride entrapped graphene aerogel; $CoCo_2O_4$ NRs/h-BN/GCE: cobalt oxide nanorods integrated hexagonal boron nitride-modified glassy carbon electrode; DPV: differential pulse voltammetry; CPT-BDD: cathodically pretreated boron-doped diamond; SWAdCSV: square-wave adsorptive cathodic stripping voltammetry. LOD: limit of detection.

Analysis of water and milk samples

The developed analytical method combining SWAdCSV and CPT-BDD was applied in the determination of RNZ in natural water samples and whole bovine milk. Table 3 presents the RNZ recovery results in fortified lake water and milk samples. The samples were enriched at two levels of analyte concentration, corresponding to the first linear range and the second linear range, respectively. According to the guidance document of the Instituto Nacional de Metrologia, Qualidade e Tecnologia (INMETRO),[67] the recovery values are considered acceptable given the low concentrations of RNZ determined in the enriched samples. The analyte concentration levels were in the order of 10^{-5}-10^{-6} mol L^{-1}, where average recovery values of 80-110% are acceptable. Therefore, evaluating the recovery percentages in Table 3, it is concluded that the proposed analytical method is applicable for the RNZ determination in lake water and milk samples. The method can be adopted, for example, as a screening tool for possible environmental contamination of water and food products by RNZ.

Table 3. Analysis of RNZ in natural water and milk samples

Sample	c(RNZ) / (μmol L^{-1})		Recovery[a] / %
	Added	Found	
Water	0.0	n.d.	–
	38.0	38 ± 2	100
	88.0	88 ± 2	100
Milk	0.0	n.d.	-
	28.0	26.9 ± 2	96.1
	85.0	82.0 ± 0.4	96.7

[a]Recovery (%) = [$c(RNZ)_{Found}/c(RNZ)_{Added}$] × 100%; c(RNZ) = molar concentration of ronizadole; n.d. = not detected.

Conclusions

A new voltammetric method was developed in this work for the determination of the antibiotic RNZ in water and milk samples using a cathodically pretreated BDD electrode. The reduction reaction of RNZ over BDD was an irreversible process, and CPT-BDD electrode was chosen to conduct the analytical tests because it provided a better voltammetric response for the analyte. Regarding the developed voltammetric method, the combination of SWAdCSV and CPT-BDD under optimal conditions provided an analytical curve with two linear concentration ranges, and LOD of 2.55 μmol L^{-1}. Validation through recovery studies demonstrated that the proposed method is satisfactory for the determination of RNZ in water and bovine milk matrice samples. The proposed voltammetric method can be explored as a RNZ screening tool in different environmental and food samples.

Supplementary Information

Supplementary information (electrochemical data) is available free of charge at http://jbcs.sbq.org.br as PDF file.

Acknowledgments

We gratefully acknowledge the Brazilian agencies CAPES (Financial code 001) and FAPEMIG (grants APQ-00083-21 and APQ-03113-22) by the financial support.

References

1. Verlicchi, P.; Galletti, A.; Petrovic, M.; Barceló, D.; *J. Hydrol.* **2010**, *389*, 416. [Crossref]
2. Khoo, Y. S.; Goh, P. S.; Lau, W. J.; Ismail, A. F.; Abdullah, M. S.; Mohd Ghazali, N. H.; Yahaya, N. K. E. M.; Hashim, N.; Othman, A. R.; Mohammed, A.; Kerisnan, N. D. A.; Mohamed Yusoff, M. A.; Hashim, N. H. F.; Karim, J.; Abdullah, N. S.; *Chemosphere* **2022**, *305*, 135151. [Crossref]
3. Ojemaye, C. Y.; Petrik, L.; *Environ. Pollut.* **2019**, *252*, 562. [Crossref]
4. Richardson, S. D.; Ternes, T. A.; *Anal. Chem.* **2018**, *90*, 398. [Crossref]
5. Marson, E. O.; Paniagua, C. E. S.; Gomes Jr., O.; Gonçalves, B. R.; Silva, V. M.; Ricardo, I. A.; V. M. Starling, M. C.; Amorim, C. C.; Trovó, A. G.; *Sci. Total Environ.* **2022**, *836*, 155605. [Crossref]
6. Couto, E.; Assemany, P. P.; Carneiro, G. C. A.; Soares, D. C. F.; *Chemosphere* **2022**, *302*, 134808. [Crossref]
7. Bell, K. Y.; Wells, M. J. M.; Traexler, K. A.; Pellegrin, M.; Morse, A.; Bandy, J.; *Water Environ. Res.* **2011**, *83*, 1906. [Crossref]
8. Xu, M.; Wang, J.; Zhang, L.; Wang, Q.; Liu, W.; An, Y.; Hao, L.; Wang, C.; Wang, Z.; Wu, Q.; *J. Hazard. Mater.* **2022**, *429*, 128288. [Crossref]
9. Polzer, J.; Stachel, C.; Gowik, P.; *Anal. Chim. Acta* **2004**, *521*, 189. [Crossref]
10. Fraselle, S.; Derop, V.; Degroodt, J.-M.; Van Loco, J.; *Anal. Chim. Acta* **2007**, *586*, 383. [Crossref]
11. Zou, X.-Y.; Lin, Y.-L.; Xu, B.; Zhang, T.-Y.; Hu, C.-Y.; Cao, T.-C.; Chu, W.-H.; Pan, Y.; Gao, N.-Y.; *Water Res.* **2019**, *160*, 296. [Crossref]
12. Hite, M.; Skeggs, H.; Noveroske, J.; Peck, H.; *Mutat. Res., Genet. Toxicol.* **1976**, *40*, 289. [Crossref]
13. Voogd, C. E.; Van Der Stel, J. J.; Jacobs, J. J. J. A. A.; *Mutat. Res., Fundam. Mol. Mech. Mutagen.* **1974**, *26*, 483. [Crossref]

14. Granja, R. H. M. M.; Nino, A. M. M.; Reche, K. V. G.; Giannotti, F. M.; de Lima, A. C.; Wanschel, A. C. B. A.; Salerno, A. G.; *Food Addit. Contam.: Part A* **2013**, *30*, 970. [Crossref]
15. Mitrowska, K.; Antczak, M.; *Food Addit. Contam.: Part A* **2017**, *34*, 573. [Crossref]
16. Polzer, J.; Gowik, P.; *Anal. Chim. Acta* **2005**, *529*, 299. [Crossref]
17. Shen, J.; Yhang, Y.; Zhang, S.; Ding, S.; Xiang, X.; *J. AOAC Int.* **2003**, *86*, 505. [Crossref]
18. Tuzimski, T.; Rejczak, T.; *J. AOAC Int.* **2017**, *100*, 1671. [Crossref]
19. Tölgyesi, Á.; Sharma, V. K.; Fekete, S.; Fekete, J.; Simon, A.; Farkas, S.; *J. Pharm. Biomed. Anal.* **2012**, *64-65*, 40. [Crossref]
20. Zhong, C.; Chen, B.; He, M.; Hu, B.; *J. Chromatogr. A* **2017**, *1483*, 40. [Crossref]
21. Liu, Z.; Wang, J.; Guo, Y.; Liu, J.; Wang, J.; Wang, C.; Wu, Q.; Wang, Z.; *J. Chromatogr. A* **2022**, *1676*, 463206. [Crossref]
22. Han, C.; Chen, J.; Wu, X.; Huang, Y.; Zhao, Y.; *Talanta* **2014**, *128*, 293. [Crossref]
23. Wang, Y.; Yuan, H.; Wan, Y.; Zhang, L.; *J. Chromatogr. A* **2022**, *1675*, 463163. [Crossref]
24. Shendy, A. H.; Al-Ghobashy, M. A.; Gad Alla, S. A.; Lotfy, H. M.; *Food Chem.* **2016**, *190*, 982. [Crossref]
25. Capitan-Vallvey, L. F.; Ariza, A.; Checa, R.; Navas, N.; *Chromatographia* **2007**, *65*, 283. [Crossref]
26. Huet, A.-C.; Mortier, L.; Daeseleire, E.; Fodey, T.; Elliott, C.; Delahaut, P.; *Anal. Chim. Acta* **2005**, *534*, 157. [Crossref]
27. Wang, Y.; He, F.; Wan, Y.; Meng, M.; Xu, J.; Zhang, Y.; Yi, J.; Feng, C.; Wang, S.; Xi, R.; *Food Addit. Contam.: Part A* **2011**, *28*, 619. [Crossref]
28. Wang, J.-H.; *J. Chromatogr. A* **2001**, *918*, 435. [Crossref]
29. Gebhardt, F.; Seuss, S.; Turhan, M. C.; Hornberger, H.; Virtanen, S.; Boccaccini, A. R.; *Mater. Lett.* **2012**, *66*, 302. [Crossref]
30. Ramos, F.; Filipe, M.; Castilho, C.; Silveira, I.; *J. Liq. Chromatogr.* **1991**, *14*, 2131. [Crossref]
31. Huang, L.; Tian, S.; Zhao, W.; Liu, K.; Guo, J.; *Talanta* **2021**, *222*, 121645. [Crossref]
32. de Faria, L. V.; Lisboa, T. P.; Campos, N. S.; Alves, G. F.; Matos, M. A. C.; Matos, R. C.; Munoz, R. A. A.; *Anal. Chim. Acta* **2021**, *1173*, 338569. [Crossref]
33. Motshakeri, M.; Sharma, M.; Phillips, A. R. J.; Kilmartin, P. A.; *J. Agric. Food Chem.* **2022**, *70*, 2427. [Crossref]
34. Simões, F. R.; Xavier, M. G. In *Nanoscience and its Applications*; Da Róz, A. L.; Ferreira, M.; Leite, F. L.; Oliveira, O. N., eds.; Elsevier: London, UK, 2017. [Link] accessed in September 2023
35. Lowinsohn, D.; Bertotti, M.; *Quim. Nova* **2006**, *29*, 1318. [Crossref]
36. Cala, P. C.; Downing Jr., G. V; Michielli, R. F.; Wittick, J. J.; *J. Agric. Food Chem.* **1976**, *24*, 764. [Crossref]
37. Diniz, J. A.; Okumura, L. L.; Aleixo, H.; Gurgel, A.; Silva, A. F. S.; *J. Environ. Sci. Health, Part B* **2020**, *55*, 583. [Crossref]
38. Karupppaiah, B.; Jeyaraman, A.; Chen, S.-M.; Huang, Y.-C.; *Electrochim. Acta* **2023**, *446*, 142008. [Crossref]
39. Stanley, M. M.; Sherlin V, A.; Wang, S.-F.; Baby, J. N.; Sriram, B.; George, M.; *J. Mol. Liq.* **2023**, *375*, 121308. [Crossref]
40. Song, C. W.; Jin, R.; Hwang, N.-M.; Kim, K. H.; *Electron. Mater. Lett.* **2019**, *15*, 630. [Crossref]
41. Einaga, Y.; *Acc. Chem. Res.* **2022**, *55*, 3605. [Crossref]
42. Kondo, T.; *Curr. Opin. Electrochem.* **2022**, *32*, 100891. [Crossref]
43. Lourencao, B. C.; Brocenschi, R. F.; Medeiros, R. A.; Fatibello-Filho, O.; Rocha-Filho, R. C.; *ChemElectroChem* **2020**, *7*, 1291. [Crossref]
44. Souza, K. A. O.; Nunes, A. M. F.; Pimentel, D. M.; Verly, R. M.; Gil, E. S.; Malagutti, A. R.; dos Santos, W. T. P.; *Electrochim. Acta* **2021**, *373*, 137891. [Crossref]
45. Oliveira, G. G.; Azzi, D. C.; Silva, T. A.; de Oliveira, P. R.; Fatibello-Filho, O.; Janegitz, B. C.; *C* **2020**, *6*, 75. [Crossref]
46. Santos, A. M.; Vicentini, F. C.; Deroco, P. B.; Rocha-Filho, R. C.; Fatibello-Filho, O.; *J. Braz. Chem. Soc.* **2015**, *26*, 2159. [Crossref]
47. Hoshyar, S. A.; Barzani, H. A. H.; Yardım, Y.; Şentürk, Z.; *Colloids Surf., A* **2021**, *610*, 125916. [Crossref]
48. Šelešovská, R.; Schwarzová-Pecková, K.; Sokolová, R.; Krejčová, K.; Martinková-Kelíšková, P.; *Electrochim. Acta* **2021**, *381*, 138260. [Crossref]
49. Sarakhman, O.; Benková, A.; Švorc, Ľ.; *Microchem. J.* **2022**, *175*, 107132. [https://doi.org/10.1016/j.microc.2021.107132]
50. Rkik, M.; Ben Brahim, M.; Samet, Y.; *J. Electroanal. Chem.* **2017**, *794*, 175. [Crossref]
51. Medeiros, A. S.; Silva, D. B.; Santos, A. O.; Castro, S. S. L.; Oliveira, T. M. B. F.; *Microchem. J.* **2020**, *155*, 104718. [Crossref]
52. Ribeiro, F. W. P.; Sousa, C. P.; Morais, S.; de Lima-Neto, P.; Correia, A. N.; *Microchem. J.* **2018**, *142*, 24. [Crossref]
53. Silva, T. A.; Pereira, G. F.; Fatibello-Filho, O.; Eguiluz, K. I. B.; Salazar-Banda, G. R.; *Diamond Relat. Mater.* **2015**, *58*, 103. [Crossref]
54. Salazar-Banda, G. R.; de Carvalho, A. E.; Andrade, L. S.; Rocha-Filho, R. C.; Avaca, L. A.; *J. Appl. Electrochem.* **2010**, *40*, 1817. [Crossref]
55. Yu, Z.; Wang, J.; Wei, Q.; Meng, L.; Hao, S.; Long, F.; *Trans. Nonferrous Met. Soc. China* **2013**, *23*, 1334. [Crossref]
56. Hutton, L. A.; Iacobini, J. G.; Bitziou, E.; Channon, R. B.; Newton, M. E.; Macpherson, J. V.; *Anal. Chem.* **2013**, *85*, 7230. [Crossref]
57. Duo, I.; Levy-Clement, C.; Fujishima, A.; Comninellis, C.; *J. Appl. Electrochem.* **2004**, *34*, 935. [Crossref]
58. Salazar-Banda, G. R.; Andrade, L. S.; Nascente, P. A. P.; Pizani, P. S.; Rocha-Filho, R. C.; Avaca, L. A.; *Electrochim. Acta* **2006**, *51*, 4612. [Crossref]

59. Suffredini, H. B.; Pedrosa, V. A.; Codognoto, L.; Machado, S. A. S.; Rocha-Filho, R. C.; Avaca, L. A.; *Electrochim. Acta* **2004**, *49*, 4021. [Crossref]
60. Tryk, D. A.; Tsunozaki, K.; Rao, T. N.; Fujishima, A.; *Diamond Relat. Mater.* **2001**, *10*, 1804. [Crossref]
61. Granger, M. C.; Swain, G. M.; *J. Electrochem. Soc.* **1999**, *146*, 4551. [Crossref]
62. Carvalho, A. E.: *Caracterização Eletroquímica de Eletrodos de Diamante Dopado com Boro em Função de seu Pré-Tratamento*; PhD Thesis, Universidade Federal de São Carlos, São Carlos, Brazil, 2007. [Crossref]
63. Holt, K. B.; Bard, A. J.; Show, Y.; Swain, G. M.; *J. Phys. Chem. B* **2004**, *108*, 15117. [Crossref]
64. Ardila, J. A.; Oliveira, G. G.; Medeiros, R. A.; Fatibello-Filho, O.; *Analyst* **2014**, *139*, 1762. [Crossref]
65. B. Oliveira, S. C.; Oliveira-Brett, A. M.; *Electrochim. Acta* **2010**, *55*, 4599. [Crossref]
66. Bard, A. J.; Faulkner, L. R.; White, H. S. In *Electrochemical Methods: Fundamentals and Applications*, 2nd ed.; John Wiley & Sons: New York, USA, 2000. [Link] accessed in September 2023
67. Instituto Nacional de Metrologia, Qualidade e Tecnologia (INMETRO); DOQ-CGCRE-008: *Orientação Sobre Validação de Métodos Analíticos,* http://www.inmetro.gov.br/Sidoq/Arquivos/Cgcre/DOQ/DOQ-Cgcre-8_05.pdf, accessed in September 2023.

Submitted: May 30, 2023
Published online: September 28, 2023